MRS Communications

https://doi.org/10.1557/s43579-021-00065-5

MRS Communications

Research Letter

Correlation between complexity and mechanical recovery of metallic nanoarchitecture structures

H. Ke, Department of Mechanical and Aeronautical Engineering, Clarkson University, Potsdam, NY 13699, USA; Additive Manufacturing Innovations LLC, Potsdam, NY 13676, USA
J. Ma, Department of Aerospace and Mechanical Engineering, Saint Louis University, Saint Louis, MO 63103, USA
I. Mastorakos, Department of Mechanical and Aeronautical Engineering, Clarkson University, Potsdam, NY 13699, USA

Address all correspondence to I. Mastorakos at **imastora@clarkson.edu**

(Received 3 May 2021; accepted 29 June 2021)

Abstract

We investigated the effect of complexity on the mechanical behavior and recovery of metallic nanoarchitecture structures. We studied four different suggested geometries with various levels of complexity using molecular dynamics simulations. The structures exhibited multiple degrees of self-recovery under compressive loading conditions at three temperatures, 300 K, 400 K, and 500 K. A methodology to qualitatively measure the geometric complexity was used. The results revealed correlations between the complexity of the structures and their recovery ability and strength, and the geometric cell size and temperature. These findings can guide the design of novel nanoarchitecture geometries for specific applications with tailored properties.

Introduction

Architected materials (cellular structures or lattice structures) have recently attracted much attention from researchers because of their exceptional mechanical properties, e.g., lightweight, high specific stiffness and strength, and excellent energy absorption capability, which are especially of interest to aerospace and automobile industries.[1–4] With the rapid development of additive manufacturing (AM) technologies, it is much easier to produce new architected structures with controlled mechanical properties for various engineering applications.

Some researchers have investigated the compression behavior of lattice structures either experimentally or numerically. Amani et al. built two face-centered cubic structures with various struts and node thicknesses by employing the selective laser melting (SLM) technique.[5] They investigated the effect of compression on the deformation of these two structures using in situ and ex situ X-ray tomography scanning. In the meantime, they established a finite element model based on 3D images and Gurson-Tvergaard-Needleman (GTN) to simulate the structures' compression tests. They revealed that the FEM model could work fairly well to predict fracture location compared with experimental results. Plocher et al. experimentally evaluated the effect of additive manufacturing parameters (density severity, unit cell size grading, and the building direction) on the structure stiffness, energy absorption, and structural response of fiber-reinforced lattices with the same relative density.[1] They observed that modest density grading had a positive effect on the stiffness of the Schwarz-P lattice and almost no impact on that of the body-centered cubic lattice. More severe grading resulted in a reduction of the total stiffness, but the SP's modulus had been higher than that of the uniform counterparts. Their experiments showed that unit cell size grading did not substantially influence the stiffness and energy absorption capability. They found an elastomer-like performance compared to a foam-like behavior of the density graded lattices of the same relative density. Their results also depicted better energy absorption capability for density grading in bending-dominated unit cell lattices if small displacements were applied; for large deformation, density grading in stretching-dominated unit cell lattices is advantageous. Dalaq et al. experimentally and analytically investigated the mechanical response of the idealized segmented system consisting of linearly arranged cubes when axial pre-compression and transverse force were applied.[6] Two failure modes (a sliding mode and a hinging mode) were identified, and the failure mode transition was built to facilitate the design of architectural structures and materials. Additionally, the authors illustrated that it was possible to delay hinging and improve stability by enriching the morphology of the cubes. Kaur et al. additively manufactured octahedral and octet microarchitectures using various polymeric materials (e.g., polylactide, nylon 618, and carbon fiber-reinforced composite) and conducted Finite Element analysis to evaluate the stress distribution in the stretching-dominating deformation of these two microstructures.[2] They revealed that nylon's octahedral and octet microstructures had comparable stiffness moduli (0.08–0.1 GPa), and the carbon fiber reinforced composite microstructures (both octahedral and

octet) showed higher modulus and energy absorption capability. Bonatti and Mohr introduced smooth shell structures as mechanical metamaterials having superior specific energy absorption capacity. They investigated experimentally and computationally the mechanical properties of the triply periodic minimal surface (TPMS)-like structure and an elastically isotropic derivate (EID).[7] They observed that substantial anisotropy for TPMS-like structures under both small and large strain conditions, and EID's mechanical properties were close to the mean value for all directions when TPMS-like structures were loaded. Their research also reported a higher mechanical performance for shell lattices than truss lattices of the same density when relative density ranges between 1 and 50% and a more stable mechanical response for shell lattices than truss lattices when relative densities exceeded 20%. Bonatti and Mohr also carried out finite element simulations to investigate the effect of relative densities between 1 and 80% on the small and large strain response of TPMS-like shell lattices.[3] They reported that highly anisotropic elastic and plastic properties depended on the type of cubic symmetry for TPMS-like shell lattices, which also possessed high specific energy absorption for large strain compression. Yin et al. used selective laser sintering (SLS) to manufacture the second-order hierarchical lattice materials of different lattice configurations and assess these materials' mechanical response in uniaxial compression. Finite element models were developed and validated against experimental results. The effect of geometrical parameters (e.g., truss aspect ratios at each level, the inclination angle) on the mechanical properties of the lattices were assessed both experimentally and numerically.[8] They showed that hierarchical octet truss with hollow mesoscopic truss members outperformed solid counterparts by 46.1% in strength. Their research also indicated that mesoscopic and macroscopic configurations positively influenced specific stiffness and failure strain, even though macroscopic configuration affected all the second-order lattice materials' specific strength. Moestopo et al. presented a new hierarchical architecture that used interwoven fibers to build effective beams, and they additively manufactured woven and monolithic lattices.[9] Their in situ tension and compression tests of these lattices revealed that the woven structures were superior to achieve 50% of both tensile and compressive strains without failure. They also reported that woven lattices exhibited a much better fatigue life than monolithic beams during cyclic compression experiments. Duan et al. experimentally and numerically assessed the elastoplastic properties and large strain response of their plate-lattices.[10] Their results showed significantly higher elastic properties in isotropic plate-lattices than conventional truss lattices and isotropic smooth shell lattices. The bulk modulus of isotropic plate-lattices could potentially reach the Hashin–Shtrikman upper bound with all relative densities. These plate-lattices exhibited remarkable energy absorption capacity under large strain conditions. Niknam and Akbarzadeh classified different types of lattices 3D printed by stereolithography according to their topology and presented an approach to improving energy absorption-to-weight ratio when these lattices were under compression conditions.[11] Their research revealed that the highest initial stiffness was obtained for the uniform design with even distribution of relative density among all 3D printed lattices. Additionally, significant enhancement of stiffness and energy absorption capacity was observed for graded design with some relative density variation under high compressive strains.

Up to now, researchers have been focusing on the material behavior of architectured structures either at millimeter-scale[1–3,5,6,8,10,11] or microscale.[7,9] In this research, we focus on the material behavior of nanoarchitecture structures with various complexities under compressive loading conditions. Atomistic modeling was carried out using molecular dynamics simulations. This paper is organized as follows: The molecular dynamics simulations methodology is described in the next section. In "Results and discussion" section, the qualitative approach to assessing structure complexity is briefly outlined, followed by the results and discussion in "Conclusions". Finally, the last "Methodology" section summarizes the conclusions of this work.

Structure complexity

First, several types of cells have been created based on typical architected structure geometries.[4,12] The use of periodic boundary conditions in all three directions allowed us to simulate large nanoarchitecture structures like those shown in Fig. 1. The systems are shown in terms of complexity starting from the least complex one. Based on the specific geometric characteristics of the structures, each unit cell possesses specific mechanical properties. These properties were obtained using molecular dynamics simulations.

The complexity of each structure was measured using the methodology described in Ref. 13. The approach was developed for studying the complexity of architectural geometric designs, and as such, it fits very well for this work. The method is based on a point system. It allocates points to geometric structures according to their complexity in seven categories: (a) geometrical complexity, (b) dimensional complexity, (c) arithmetic of shapes, (d) transformations, (e) number of shapes, (f) shape of elements, and (g) color. The last category was not included in our evaluation of the structural complexity as it is not relevant to the present work. The final complexity score for each structure was normalized with the more complex design score to compare better how far each structure was from the most complex one.

Based on this approach, the most complex structure was the structure (D), followed by structures (C) and (B) of Fig. 1. Structures (C) and (D) scored very close, with structure (D) achieving the higher score due to its curved links. The first structure in Fig. 1, structure (A), was the least complex, with a normalized score of 0.25 or only 25% as complex as the most complex structure.

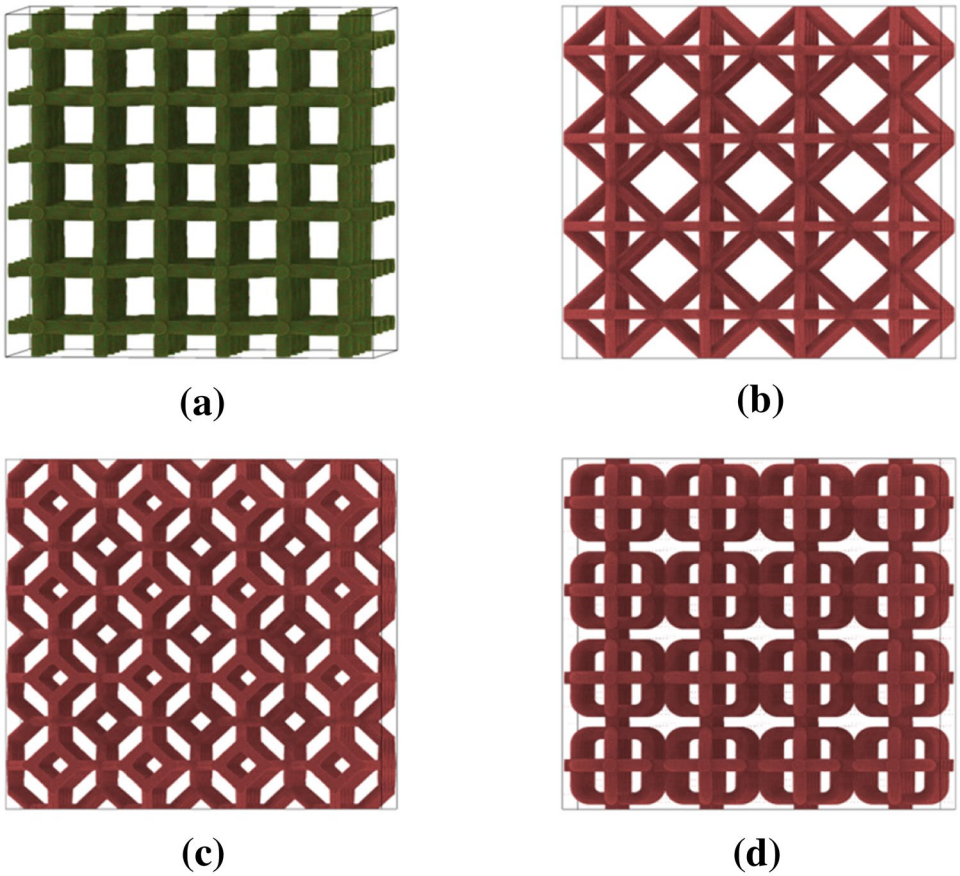

Figure 1. The four structures studied in this work.

Results and discussion

The loading and unloading of all the structures in Fig. 1 resulted in obtaining their stress–strain curves. A characteristic curve is shown in Fig. 2(a). All structures exhibited similar stress–strain curves. The small differences observed in the plastic regions of the stress–strain curves for the same box sizes loaded to different maximum strains, are due to the stochastic nature of the thermal vibrations added in the molecular dynamics through the random number generator. These differences, although visible, they all fall in the same ranges for the same box sizes and they are not affecting the conclusions. The pseudoelastic recovery strain is defined as the extra strain recovered during unloading after the elastic strain has been subtracted. The term "pseudoelastic" was borrowed from a similar behavior exhibited when very thin nanowires recover fully after the plastic region has been reached during uniaxial loading.[14,15] We found the

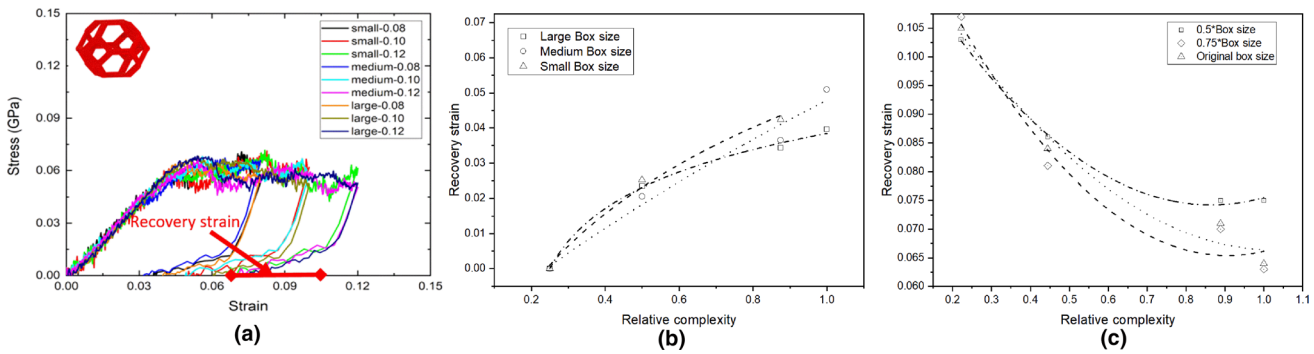

Figure 2. (a) Loading–unloading stress–strain curves for structure (A) at 400 K at three different maximum strains, 8%, 10%, and 12%. All four structures produced similar stress–strain curves. The box sizes denoted large, medium, and small are for the 100%, 75%, and 50% of the original box size. The recovery strain is shown in the red arrow. The inset shows the colors of the stress–strain curves for different box sizes, loaded up to different total strains. (b) The effect of the structural complexity on the total recovery strain for the temperature of 300 K. Similar trends were observed in the other two temperatures. (c) Yield stress dependence on the relative complexity.

pseudoelastic strain to be characteristic of the structure and depend on the complexity of the geometry. However, it should be pointed out that the mechanisms responsible for this behavior are not the same as in the very thin nanowires. The recovery ability is related to the shape and geometry of the structures rather than a phase transformation process as in nanowires. As will be discussed below, this phase transformation hinders the recovery behavior rather than enhancing it.

The effect of the geometric complexity on the pseudoelastic recovery (termed recovery strain for simplicity from now on) is shown in Fig. 2(b). The results reveal that the value of pseudoelastic strain increases as the complexity of the structure increases. However, this increase is not monotonous and seems to saturate as the structure becomes more complex.

Also, the effect of the complexity on the yield stress of the structures was studied. The results for the 300 K are shown in Fig. 2(c). Similar trends are found for all the other temperatures. The least complex structures exhibited the higher yield stress. As the structure becomes more complex, the yield stress drops. By observing the geometries of the structures, it is clear that the last system (the most complex one) is the only one with curved ligaments that seem to facilitate the initiation of plastic deformation and thus the drop in yield stress. This is more evident when comparing structures (B) and (D). These structures are similar except that the second structure has straight ligaments while the fourth has curved ones. However, the straight ligaments' structure is about 25% stronger than the structure with the curved ligaments, which also happens to be the most complex one.

From Fig. 2(b), the recovery strain is affected by the box size only in the last three more complex structures, with the smaller structures exhibiting higher recovery strains. The opposite effect seems to occur in the yield stress in Fig. 2(c), where the least complex structure exhibits the larger dependence on the box size, decreasing as the structure becomes more complex. The large change in the yield stress observed in the least complex structure can be attributed on the presence of only horizontal and perpendicular ligaments that exhibits only pure compression compared to the other structures that exhibit more complex loadings. The yield stress dependence that is more obvious in the case of the least complex structure is typical to that observed in cylindrical ligaments of small thicknesses. In these cases, the yield strength reduces as the size decreases. This effect has been reported for fcc nanowires and is attributed to the shape of the ligaments.[16–18] In the case of the more complex structures, these trends are not very obvious, and this can only be an effect of the geometry, especially since no dislocation interaction mechanisms of any importance were observed. For the second and third more complex structures, the similar yield stresses can only be caused by their geometries. These two structures have both ligaments along a similar angle with the loading direction, and as such, the dislocations nucleate at the same stress, and in the same locations, which are at the joints of ligaments.

The recovery is more intense as the box size decreases, and as a consequence, the ligament cross-sectional area decreases [Fig. 3(a)]. This result agrees with the findings for metal nanowires, which report a higher pseudoelastic strain for thinner nanowires.[19] This behavior is limited to very thin ones (at thicknesses ~ 1.5 nm for square cross-sections) and dies out very fast.[20] In this case, the recovery continues at thicknesses much higher than in single nanowires, and it can be attributed to the geometric complexity of the nanostructures. It becomes apparent when comparing the geometry of the most simple structure (structure (A) in Fig. 1) to that of the nanowires. This structure is made of horizontal and vertical ligaments, which are very similar to the simple nanowires. The thickness of the ligaments of the smaller structure is higher than the critical thickness for a single metal nanowire to exhibit pseudoelasticity, and as such, the pseudoelastic recovery is negligible. However, this is not the case in the more complex structures, where even the thicker ligaments, well above the critical thickness for pseudoelasticity, exhibit recovery, although partial. The simulations revealed that more dislocations nucleated at the joints of the ligaments in the three least complex structures, although no specific deformation mechanisms in any structures other than

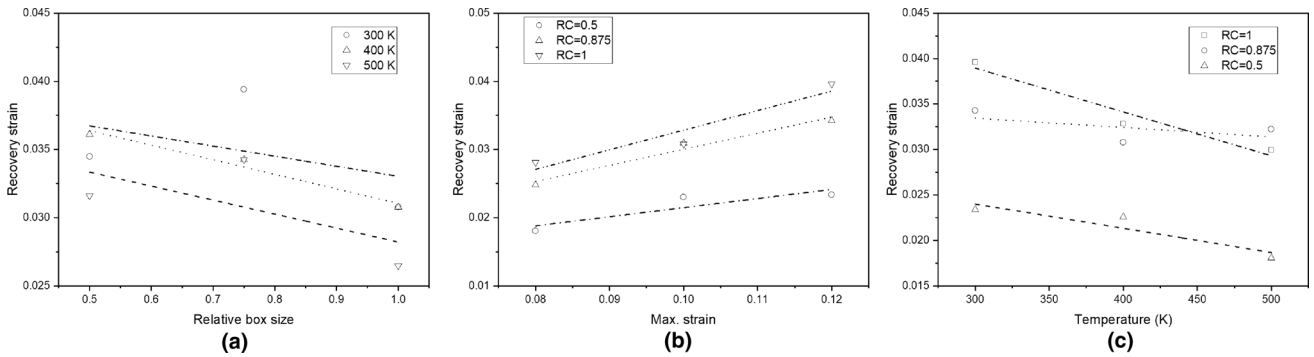

Figure 3. (a) The recovery strain as a function of the relative box size at the three temperatures, 300 K, 400 K, and 500 K. for structure (C). Similar behavior is exhibited for other shapes except for structure (A). (b) The recovery strain is plotted against the maximum loading strain for the three structures that exhibit recovery. (RC = relative complexity). (c) The effect of the temperature in the structure recovery for the case of 12% maximum strain loading. Similar trends were observed for the other two maximum loading strains.

the nucleation and propagation of dislocations inside the ligaments were observed. This observation led us to conclude that the complexity of the structures is responsible for this observed behavior since it is directly related to the shape of the unit cells.

The extent of the recovery ability of a structure was also tested by loading and unloading the structure up to three different final strains, 8, 10, and 12%. The results for the temperature of 300 K are shown in Fig. 3(b). Similar trends were observed in all temperatures. It appears that the most complex structure has the better ability to recover even at high strain, as the increasing slope of the linear fitting suggests. This is attributed once again to the geometry of the structures and the interconnection of the ligaments that allow the structures to return close to their original shape. The presence of curved ligaments in structure (D) is the critical factor that results in higher recovery by preventing or limiting the ability of dislocations nucleate or moving to the free surface and thus causing permanent deformation.

The effect of the temperature on the recovering ability of the structures is shown in Fig. 3(c). In this case, the recovery strain is decreasing as the temperature increases. This can be attributed to two factors: (a) the reduction of the stiffness of the structures with the increase of temperature that makes them "softer," and therefore easier to remain in the deformed configuration, and (b) to the higher dislocation content, resulting from the reduced stiffness, that also makes the pseudoelastic recovery more difficult. This is more evident in the case of the most complex structure, where the reduction in stiffness is more significant, probably due to the presence of the curved ligaments. The reduction of stiffness in the last structure (D) from 300 K to 500 K is approximately 20%. In the other three structures, the reduction is 13%, 14%, and 13% for structures (C), (B), and (A), respectively.

In all loading cases, structure (A) did not experience any recovery strain. This is attributed to the different deformation behavior that this structure exhibits compared to the other three and underlines the importance of the geometry in the overall process. Details of the deformation of the structure (A) are shown in Fig. 4.

The unit cell of structure (A) with straight perpendicular ligaments exhibited a deformation behavior based on the nucleation and propagation of multiple twin boundaries occurring during compression, as shown in Fig. 4(e). During the compression, the original ligament configuration of $\langle 001 \rangle / \{100\}$ is transformed to ligaments with mixed configurations of $\langle 001 \rangle / \{100\}$ and $\langle 110 \rangle / \{111\}$ (Fig. 4f). This process can lead to

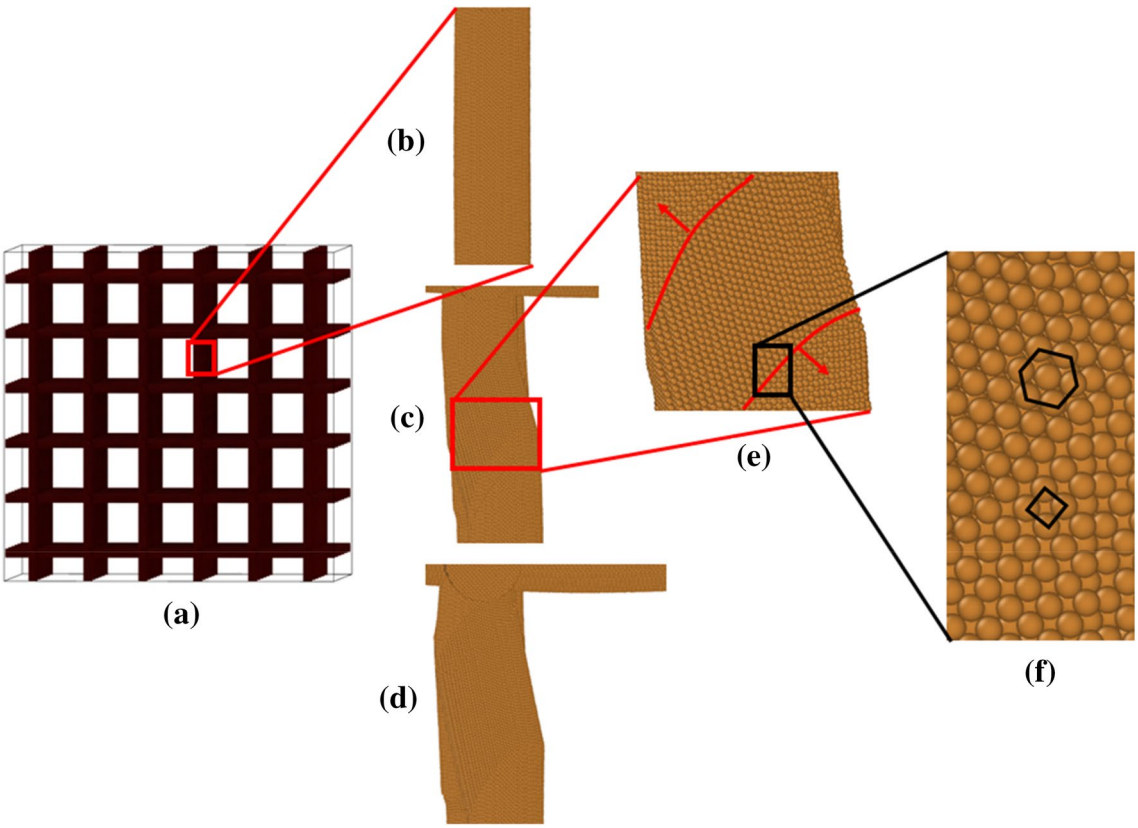

Figure 4. (a) The original structure (A). (b), (c) and (d) a magnification of a region highlighted by the red box in (a). (b) initial structure, (c) the structure in the middle of the loading, and (d) the structure after the unloading. (e) A magnification of the area of the red box in (c). The twinning region is between the two red lines, and the arrows show the direction of propagation. (f) Magnification of the area in the black box in (e). These two discrete atomic orientations are indicated with the black hexagon and square, respectively.

complete recovery of the original ligaments in small ligament thicknesses (below 2–3 nm at 300 K).[20,21] However, in thicker ligaments, the process is not reversible, resulting in the permanent deformation observed in structure (A). Only the ligaments of structure (A) exhibited this behavior. In all other structures, ligaments in non-perpendicular directions resulted in buckling that assisted their partial recovery. This behavior has also been observed in nanowires under compression. One reason is the low dimension of the structure. Another reported reason may be the movement of the ligaments at the end supports, as perfect rigid support is impossible.[22] In various directions and angles, the presence of many ligaments with respect to the loading direction in the most complex structures facilitated the recovery process leading to higher recovery strains. Further analysis of this mechanism is required to understand this effect and its limitations. This analysis is beyond the scope of this paper, and it will be addressed in a separate work.

Conclusions

In this work, we discussed how the complexity of nanoarchitecture metallic structures affects their mechanical properties. We suggested a methodology derived from the architectural geometric designs that we applied to measure the complexity of four structures. Then we performed molecular dynamics simulations to evaluate the mechanical properties of these structures. The results reveal a correlation between the complexity of the structures and their self-recover ability after extreme compressive loading. Our findings suggest that the most complex structures exhibit higher self-recovery under compression, and therefore are more reliable for applications where the compressive stresses can become significant. However, the results also suggest that the most complex structure is the least strong, as the yield stress tends to decrease as the complexity increases. The results can guide the design of nanoarchitecture structures for specific applications, where the decision must be based on which property is more important, e.g., recovering ability or strength. The recovery capacity increases as the ligament size decrease, in accordance with similar findings on pseudoelastic nanowires. Finally, the effect of the temperature was investigated, and it was found that as the temperature increases, the capability of recovery decreases because the structures become softer. In this case, the more substantial decrease is exhibited by the most complex structure, revealing the limitations of these geometries.

Methodology

In all our simulations, we used copper atoms because of their reliable interatomic potentials and broad potential applications. All four structures have similar porosities to eliminate its effect from the mechanical properties and focus only on the influence of the structural complexity.

First, a simulation box of 15 nm × 15 nm × 15 nm containing copper atoms with (001) direction was formed. The geometries of the unit cells were first produced in SolidWorks and exported in standard tessellation language (TSL) format that records only the surface geometry of a structure. The files were then imported into Atomsk[23] to fill the interior of the surfaces with atoms. Special care was placed to ensure that the boundary elements of the structures would be drawn in such a way as to fit well with the opposite parts to maintain the periodicity of the unit cells, as in Ref. 24. The radius of the individual ligament in the original boxes was kept at 3 nm for all the unit cells. The number of atoms in the different configurations and box sizes was approximately the same, with minor variations due to different geometries. The size of the simulation boxes in all unit cells was the same, resulting in similar porosities in the range of 7–13% for all cases. It also affected the thickness of the ligaments in the medium and small boxes that were reduced accordingly (by ~ 25% and 50%, respectively). The similar porosity allowed us to exclude its effect from our discussion and focus only on the complexity of the structures, as the minor variations used in this work were not enough to alter the results considerably. The molecular dynamics simulations were performed using LAMMPS[25] and the embedded atom method (EAM) Voter and Chen interatomic potentials.[19,26,27] The structures' energy was first relaxed using a Conjugate Gradient method and then brought to the desired temperature for thermal relaxation. In this work, three different temperatures were studied, e.g., 300 K, 400 K, and 500 K. Then the structures were loaded uniaxially under compression along the y-direction at a strain rate of $-5 \times 10^9 s^{-1}$ at a constant temperature of 300 K. The high strain rate is a characteristic of the molecular dynamics simulations due to the low time scale, which in our simulations was 1 fs. Although lower strain rates will change the quantitative characteristics of the stress–strain curves, they would not alter their relative qualitative values concerning the other structures, e.g., the stronger structure would still be stronger, even though demonstrating lower yield stress. Therefore, as the purpose of this work is to compare how structures of various complexities behave with respect to each other, the value of the strain rate used is not critical, and the qualitative results presented in this work are still valid. The same holds for the effect of the box size. A change in box size alters the results quantitatively and not qualitatively, and therefore, a convergence study was not necessary and not conducted. The isothermal-isobaric (NPT) ensemble was used to update the atomic velocities and positions at each step. After a specific strain has been reached, the loading was removed, and the structures were allowed to relax. Three maximum strains were used (8%, 10%, and 12%) before the structures relaxed.

Acknowledgments

H.K and I.M. would like to acknowledge the support of the National Science Foundation under Grant No. CMMI-MEP-1634640. Some of the computing for this work was performed on the ACRES cluster funded by the National Science

Foundation under Grant No. 1925596. H.K. and I.M. would like to thank the N.S.F. and Clarkson University's Office of Information Technology for providing computational resources and support that contributed to these research results. J. M. would like to thank Saint Louis University's Research Computing Group for providing HPC resources and support to run some of the MD simulations.

Declarations

Conflict of interest

On behalf of all authors, the corresponding author states that there is no conflict of interest.

References

1. J. Plocher, A. Panesar, Effect of density and unit cell size grading on the stiffness and energy absorption of short fibre-reinforced functionally graded lattice structures. *Addit. Manuf.* **33**, 101171 (2020). https://doi.org/10.1016/j.addma.2020.101171
2. M. Kaur, T.G. Yun, S.M. Han, E.L. Thomas, W.S. Kim, 3D printed stretching-dominated micro-trusses. *Mater. Des.* **134**, 272–280 (2017). https://doi.org/10.1016/j.matdes.2017.08.061
3. C. Bonatti, D. Mohr, Smooth-shell metamaterials of cubic symmetry: anisotropic elasticity, yield strength and specific energy absorption. *Acta Mater.* **164**, 301–321 (2019). https://doi.org/10.1016/j.actamat.2018.10.034
4. J.R. Greer, V.S. Deshpande, Three-dimensional architected materials and structures: design, fabrication, and mechanical behavior. *MRS Bull.* **44**, 750–757 (2019). https://doi.org/10.1557/mrs.2019.232
5. Y. Amani, S. Dancette, P. Delroisse, A. Simar, E. Maire, Compression behavior of lattice structures produced by selective laser melting: X-ray tomography based experimental and finite element approaches. *Acta Mater.* **159**, 395–407 (2018). https://doi.org/10.1016/j.actamat.2018.08.030
6. A.S. Dalaq, F. Barthelat, Strength and stability in architectured spine-like segmented structures. *Int. J. Solids Struct.* **171**, 146–157 (2019). https://doi.org/10.1016/j.ijsolstr.2019.04.012
7. C. Bonatti, D. Mohr, Mechanical performance of additively-manufactured anisotropic and isotropic smooth shell-lattice materials: simulations & experiments. *J. Mech. Phys. Solids* **122**, 1–26 (2019). https://doi.org/10.1016/j.jmps.2018.08.022
8. S. Yin, H. Chen, J. Li, T.X. Yu, J. Xu, Effects of architecture level on mechanical properties of hierarchical lattice materials. *Int. J. Mech. Sci.* **157–158**, 282–292 (2019). https://doi.org/10.1016/j.ijmecsci.2019.04.051
9. W.P. Moestopo, A.J. Mateos, R.M. Fuller, J.R. Greer, C.M. Portela, Pushing and pulling on ropes: hierarchical woven materials. *Adv. Sci.* **7**, 2001271 (2020). https://doi.org/10.1002/advs.202001271
10. S. Duan, W. Wen, D. Fang, Additively-manufactured anisotropic and isotropic 3D plate-lattice materials for enhanced mechanical performance: simulations & experiments. *Acta Mater.* **199**, 397–412 (2020). https://doi.org/10.1016/j.actamat.2020.08.063
11. C. Gao, W. Wu, J. Shi, Z. Xiao, A.H. Akbarzadeh, Simultaneous enhancement of strength, ductility, and hardness of TiN/AlSi10Mg nanocomposites via selective laser melting. *Addit. Manuf.* **34**, 101378 (2020). https://doi.org/10.1016/j.addma.2020.101378
12. M.F. Ashby, A.G. Evans, N.A. Fleck, L.J. Gibson, J.W. Hutchinson, H.N.G. Wadley, *Metal Foams: A Design Guide* (Butterworths, London, 2000)
13. A.A. Globa, M. Donn, O.A. Ulchitskiy, Metrics for measuring complexity of geometric models. *Scientific visualization* **8**(5), 74–82 (2016)
14. X. Guo, W. Liang, M. Zhou, Mechanism for the pseudoelastic behavior of FCC shape memory nanowires. *Exp. Mech.* **49**, 183–190 (2009). https://doi.org/10.1007/s11340-008-9173-x
15. I.N. Mastorakos, H.M. Zbib, D.F. Bahr, J. Parsons, M. Faisal, Pseudoelastic behavior of Cu-Ni composite nanowires. *Appl. Phys. Lett.* **94**, 043104 (2009). https://doi.org/10.1063/1.3073984
16. J. Marian, J. Knap, Breakdown of self-similar hardening behavior in Au nanopillar microplasticity. *JMC* (2007). https://doi.org/10.1615/IntJMultCompEng.v5.i3-4.100
17. Y. Gan, J.K. Chen, Molecular dynamics study of size, temperature and strain rate effects on mechanical properties of gold nanofilms. *Appl. Phys. A* (2009). https://doi.org/10.1007/s00339-008-4970-8
18. H. Ke, I. Mastorakos, Deformation behavior of core–shell nanowire structures with coherent and semi-coherent interfaces. *J. Mater. Res.* **34**, 1093–1102 (2019). https://doi.org/10.1557/jmr.2018.491
19. A.F. Voter, *Intermetallic Compounds. Principles and Practice* (Wiley, Chichester, 1995)
20. H. Park, K. Gall, J. Zimmerman, Shape memory and pseudoelasticity in metal nanowires. *Phys. Rev. Lett.* **95**, 255504 (2005). https://doi.org/10.1103/PhysRevLett.95.255504
21. W. Liang, M. Zhou, Pseudoelasticity of single crystalline Cu nanowires through reversible lattice reorientation. *J. Eng. Mater. Technol. Trans. ASME* **127**, 423–433 (2005)
22. M. Riaz, O. Nur, M. Willander, P. Klason, Buckling of ZnO nanowires under uniaxial compression. *Appl. Phys. Lett.* **92**, 103118 (2008). https://doi.org/10.1063/1.2894184
23. P. Hirel, Atomsk: a tool for manipulating and converting atomic data files. *Comput. Phys. Commun.* **197**, 212–219 (2015). https://doi.org/10.1016/j.cpc.2015.07.012
24. H. Ke, A.G. Jimenez, D.A.R. Da Silva, I. Mastorakos, Multiscale modeling of copper and copper/nickel nanofoams under compression. *Comput. Mater. Sci.* **172**, 109290 (2020). https://doi.org/10.1016/j.commatsci.2019.109290
25. S.J. Plimpton, Fast parallel algorithms for short-range molecular dynamics. *J. Comput. Phys.* **117**, 1–19 (1995)
26. M. Daw, M. Baskes, Embedded-atom method: derivation and application to impurities, surfaces, and other defects in metals. *Phys. Rev. B* **29**, 6443–6453 (1983)
27. A.F. Voter, S.P. Chen, Accurate Interatomic Potentials for Ni, Al and Ni3Al, MRS Online Proceedings Library (OPL). **82** (1986). https://doi.org/10.1557/PROC-82-175